Theoretical and Applied Climatology (2022) 150:405–423
https://doi.org/10.1007/s00704-022-04145-x

ORIGINAL PAPER

Assessment of paddy expansion impact on regional climate using WRF model: a case study in Sanjiang Plain, Northeast China

Peng Huang[1] · Dan Li[1] · Hua Xie[1] · Chaoli Liu[2] · Hayat Ullah[3] · Yang Xu[4] · Changhong Song[5] · Chunsheng Dai[5] · Yuanlai Cui[1] · Yufeng Luo[1]

Received: 28 February 2022 / Accepted: 13 July 2022 / Published online: 11 August 2022

Abstract

Paddy expansion changes land use types and increases irrigation, which results in altering surface-atmosphere energy flux exchange processes with an additional impact of increase in temperature. The paddy fields have expanded approximately 14 times in the Sanjiang Plain since the 1990s. The main conversion sources for this expansion are dryland, wetland, and woodland. This expansion in paddy area induced by different sources has an integrated effect on regional climate that may produce warming or cooling effect, with different intensities in different zones. In this study, two numerical experiments (case A and case B) were designed to simulate the impacts of paddy expansion on temperature and energy flux by using the Weather Research and Forecasting (WRF) model. Irrigation cannot be ignored that it is considered a unique agricultural management measure for paddy field compared to other land covers. And considered to depict paddy expansion process accurately, multiple remote sensing-based vegetation indexes, such as green vegetation fraction (GVF) and surface albedo (ALB) were incorporated to specify the vegetation properties induced by paddy expansion. Hegang concentrated expansion zones (HGCE), Fuyuan concentrated expansion zones (FYCE), Tongjiang concentrated expansion zones (TJCE), and Sanjiang Plain expansion zones (SJPE) were selected for this research. The results revealed that paddy expansion decreased the near-surface temperature. Cumulative temperature declined by 0.80 °C (HGCE), 0.61 °C (FYCE), 0.69 °C (TJCE), and 0.43 °C (SJPE) from June to September with more significant near-surface cooling in summer (July and August). In terms of energy balance, an increase in latent heat (LH) and ground heat flux (G) and a decrease in sensible heat (SH) were observed, but the impact of paddy expansion was more significant on LH, followed by SH and G, respectively. This study provides valuable information for future agricultural activities adjustment and mitigating climate change at the regional scale.

1 Introduction

Agricultural expansion is defined as the natural vegetation converted to agricultural land (Arvor et al. 2012), was driven by diet, population, yield, and bioenergy (Alexander et al. 2015). Agricultural expansion is one of the major land use changes on a global scale, including land use cover change (LUCC) and land use management changes (LUMC), such as irrigation and fertilization (Lobell et al. 2008). The regional climate is affected by LUCC and LCMC (Bright et al. 2017). LUCC is a great contributor to global climate change by demonstrating the effect of anthropogenic forcing on Earth's surface (Feddema et al. 2005; Brian 2009; Mccarl et al. 2014; Zhang et al. 2016; Li et al. 2020). LUMC regulates the microclimate by affecting radiation balance, turbulent exchange, evaporative heat dissipation, greenhouse gas emissions, and others, which in turn affects regional climate (Intergovernmental Panel on Climate Change (IPCC)

✉ Yufeng Luo
yfluo@whu.edu.cn

[1] State Key Laboratory of Water Resources and Hydropower Engineering Science, Wuhan University, Wuhan 430072, Hubei, China

[2] Fujin City Water Affairs Bureau, Fujin 156100, Heilongjiang, China

[3] Department of Food, Agriculture and Bioresources, School of Environment, Resources and Development, Asian Institute of Technology, Pathum Thani 12120, Thailand

[4] Inner Mongolia Water Conservancy Research Institute, Hohhot 010051, Inner Mongolia, China

[5] Heilongjiang Water Conservancy Investment Group Co. Ltd, Harbin 150080, Heilongjiang, China

2001; Gregory et al. 2002; Gibbard et al. 2005; Betts et al. 2007; Thiery et al. 2017; Kang and Eltahir, 2019; Nocco and Smail 2019). A case study over eastern Amazonia stated that precipitation reduced about 24%, sensible heat fluxes increased by 54%, and latent heat decreased by 31% due to soybean cropland expansion (Sampaio et al. 2007). Liu et al. (2018) revealed an average monthly temperature warming up to 1.31 °C induced by reclaiming wetlands into dryland, and a cooling effect of 1.32 °C triggered by dryland converted to paddy fields.

Paddy expansion is rooted mainly in reclamation (wetland, forest) and dryland conversion in Sanjiang Plain (Liu et al. 2018), which is mainly embodied in changes of land use types and irrigation (Lobell et al. 2008). According to energy balance and land surface bio-geophysical characteristics, climate changes are the result of land surface energy redistribution, which are affected by surface albedo, heat capacity, roughness, and energy flux (Burkett and Kusler 2000; Anderson et al. 2003; Kueppers et al. 2007; Erwin 2009; Puma and Cook, 2010; Yu et al. 2014). Paddy expansion cause critical changes in parameters needed for land surface energy balance equation, including surface albedo, leaf area index, and fractional vegetation cover (Lee et al. 2011; Bright et al. 2017). The surface albedo plays a key role in influencing radiation and energy balance (Burakowski et al. 2018) and perturbates the radiation budget of Earth that is a fundamental climate system driver (Betts et al. 2007). Changes in leaf area index affect latent heat transport energy, impacting the temperature. Green vegetation fraction directly determines surface albedo influencing the interaction between the surface and the atmosphere (Dan et al. 2007). In addition, paddy expansion inevitably resulted in significantly increase irrigation water that is considered as first-order climate forcing factor (Kueppers et al. 2007). Other climatic impacts due to irrigation includes reduce temperature and wind speed, with an increase humidity and precipitation in agricultural areas (Bonfils and Lobell 2007; Jodar et al. 2010; Mao et al. 2011; Jia et al. 2016; Zhao et al. 2016; Han et al. 2018). In terms of the realistic background and mechanism analysis, modeling the effects of paddy expansion on regional climate with precise details is essential to make certain ET_o (Hu et al. 2021).

Previous studies have been conducted in the Sanjiang Plain, which were mainly focused on revealing the temperature effects triggered by paddy expansion based on analyzing merely remote sensed products (Liu et al. 2018; Liu et al. 2019; Du et al. 2019). Liu et al. (2018) revealed a near-surface cooling in spring (May and June), summer (July and August) and autumn (September), which was − 2.03 K, − 0.73 K, and − 1.08 K, respectively. Du et al. (2019) found that land surface temperature changes ranged from 0.6 to 5.1 °C between the high and low levels from May to October. However, remote sensing data was unable to exclude the effect of global climate warming, and the trend of energy fluxes is still unclear due to lack of research on energy fluxes. The WRF model is a next-generation mesoscale numerical weather prediction system that serves as atmospheric research and operational forecasting, which has been proven to have a solid application foundation and trustworthy simulation effects on the aspect of climate simulation. It was with the support of the WRF model that quantified effects of land use conversion and human behavior on regional climate have been captured extensive attention, such as urbanization (Li et al. 2013; Su et al. 2021), deforestation (Bala et al. 2007; Lee et al. 2011), vegetation greening (Bai et al. 2019; Yu et al. 2020), agricultural expansion (Zhang et al. 2018), and irrigation (Jiang et al. 2014; Wu et al. 2018; Liu et al. 2021a, b). Yu et al. (2021) applied the WRF model and found that T-2 m temperature decrease by 0.27 to 0.67 °C, and Rh-2 m increased by 0.94 to 2.35% due to paddy plant on saline-alkali land from June and September. Conversion to irrigated agriculture resulted in latent heat flux increase by 12.10 Wm^{-2}, sensible heat fluxes decrease by 8.85 Wm^{-2} by using the WRF model (Jiang et al. 2014). Although many studies simulate the regional climate impacts based on the WRF model, which were mainly focused on a specific land use change or agricultural irrigation, attention has rarely been paid to the integrated effects of other land converted to paddy fields.

The Sanjiang Plain used to be known as the "Great Northern Wilderness" because it was a floodplain with the largest swamps in China (Yan et al. 2018). Today, it is called "Great Northern Granary" and has become a vital high-quality commodity grain production base, where has experienced wetland reclamation and dryland development over the past seven decades (Liu et al. 2019). With the support of food policy, agricultural development, and global warming (Gao and Liu 2011; Chen et al. 2018), paddy expansion phenomenon of "northward and eastward" in the Sanjiang Plain has emerged (Zhang et al. 2017a, b), where paddy cultivation area increased approximately 14 times from 1986 to 2018 and reached an average rate of 73.94 million hectares per decade (Gao et al. 2020). It is valuable to study the effect of increased paddy cultivation considering regional climate controls evapotranspiration, which affects ET_0 (Luo et al. 2018; Dong et al. 2021; Hu et al. 2021). The positive impacts of paddy expansion on agricultural development and food security have become more far-reaching, while agricultural restructuring and water demand are definitely contradictory to eco-economic benefits. In the Sanjiang plain where paddy expanded rapidly and extensively, the regional climate effects of paddy expansion have not been quantified precisely. And few studies have paid attention to differential impacts in different regions and scale effects due to paddy expansion in this plain.

In this work, we aimed for quantifying the impacts of energy flux and temperature, explore the regional climate responses mechanisms due to the vegetation change induced by paddy expansion. This study presented the typicality of selecting paddy expansion zones, the profundity of analyzing regional differentiation effects, and the creativity of simulating paddy expansion triggered by multiple land use types converted together to paddy fields based on the WRF model. The objectives are as follows: (a) evaluate the performance of the WRF model to simulate paddy expansion in Sanjiang Plain, (b) quantify the effects of paddy expansion on energy flux and temperature, and (c) explore the responses mechanisms that different expansion zones produce differentiated effects.

2 Materials and methods

2.1 Study area

The study area is located in the Sanjiang Plain in northeastern Heilongjiang Province, China. Sanjiang Plain lies between 43°49′N–48°27′N north latitude and 129°11′E–135°05′E longitude (Fig. 1), covering an area of approximately 1.09×10^5 km^2, with a general topography of high southwest and low northeast. The area is characterized by a temperate humid and semi-humid continental monsoon climate, where annual precipitation is 500 ~ 650 mm (more than 70% of which is received in the summer monsoon from June to September). The annual average temperature is 1 ~ 4 ℃, while average summer temperature is above 22 °C, which is suitable for crops growth.

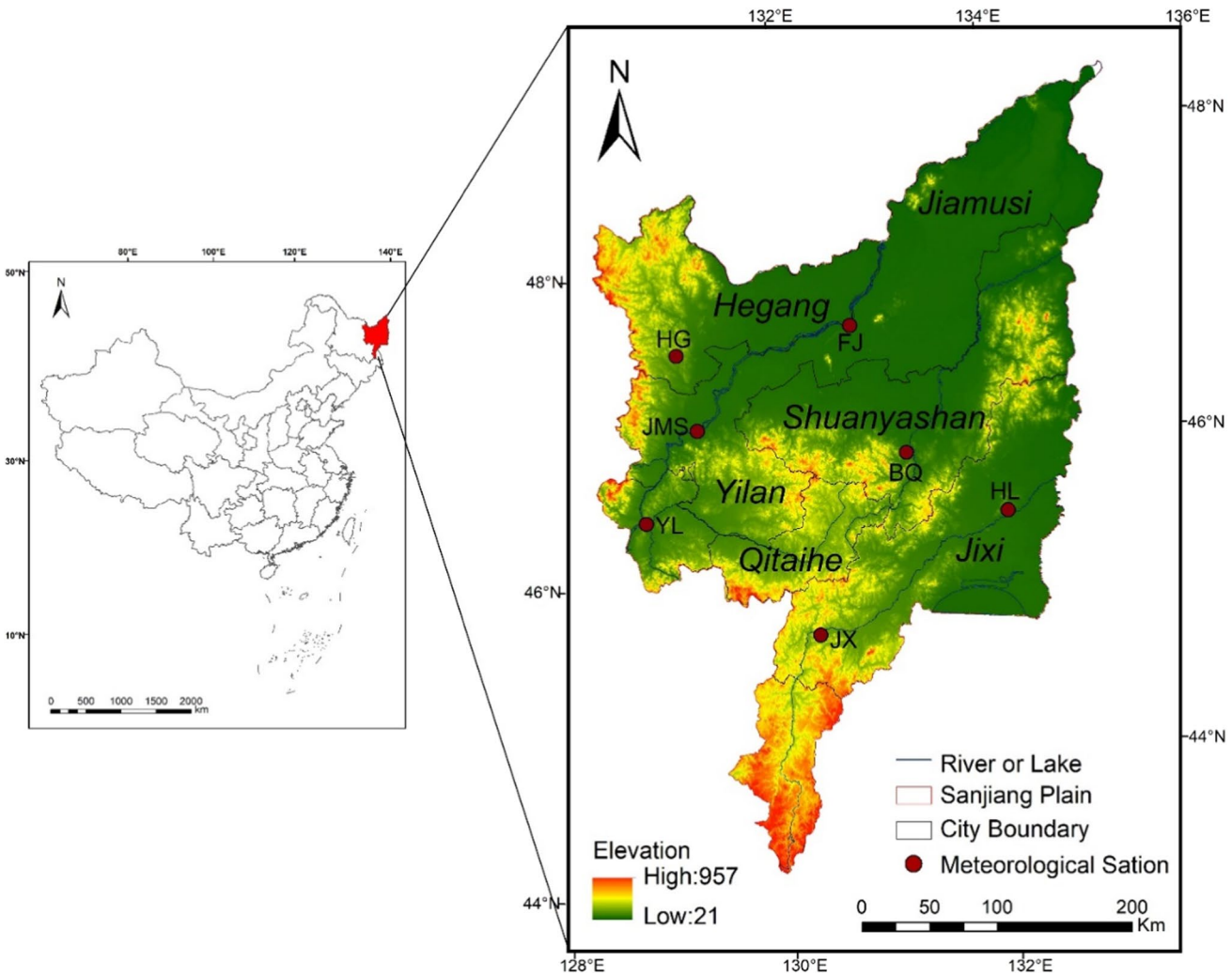

Fig. 1 Location of the study area—the Sanjiang Plain

The paddy growth period in this area is June to September. In the past two decades, large-scale "reclamation" and "conversion of dryland to paddy field" have been carried out in the Sanjiang Plain, resulting in a continuous expansion of the paddy cultivation area. From 2000 to 2018, the phenomenon of "northward and eastward expansion" and the characteristics of regional concentration in the Sanjiang Plain has emerged (Fig. 2). According to the administrative regions, we found that paddy expansion was mainly concentrated in two cities (Hegang and Jiamusi), while Jiamusi city was concentrated in Fujin, Fuyuan, and Tongjiang counties. To explore the relationship between paddy expansion ratio and regional climate change, the zones with different expansion ratio was deserved to study. And the purpose was explored the effect of merely paddy expansion, the zones where paddy expansion was concentrated excluded other land use change types. We selected three concentrated expansion zones for our work, included Hegang concentrated expansion zones (HGCE), Fuyuan concentrated expansion zones (FYCE), and Tongjiang concentrated expansion zones (TJCE), which

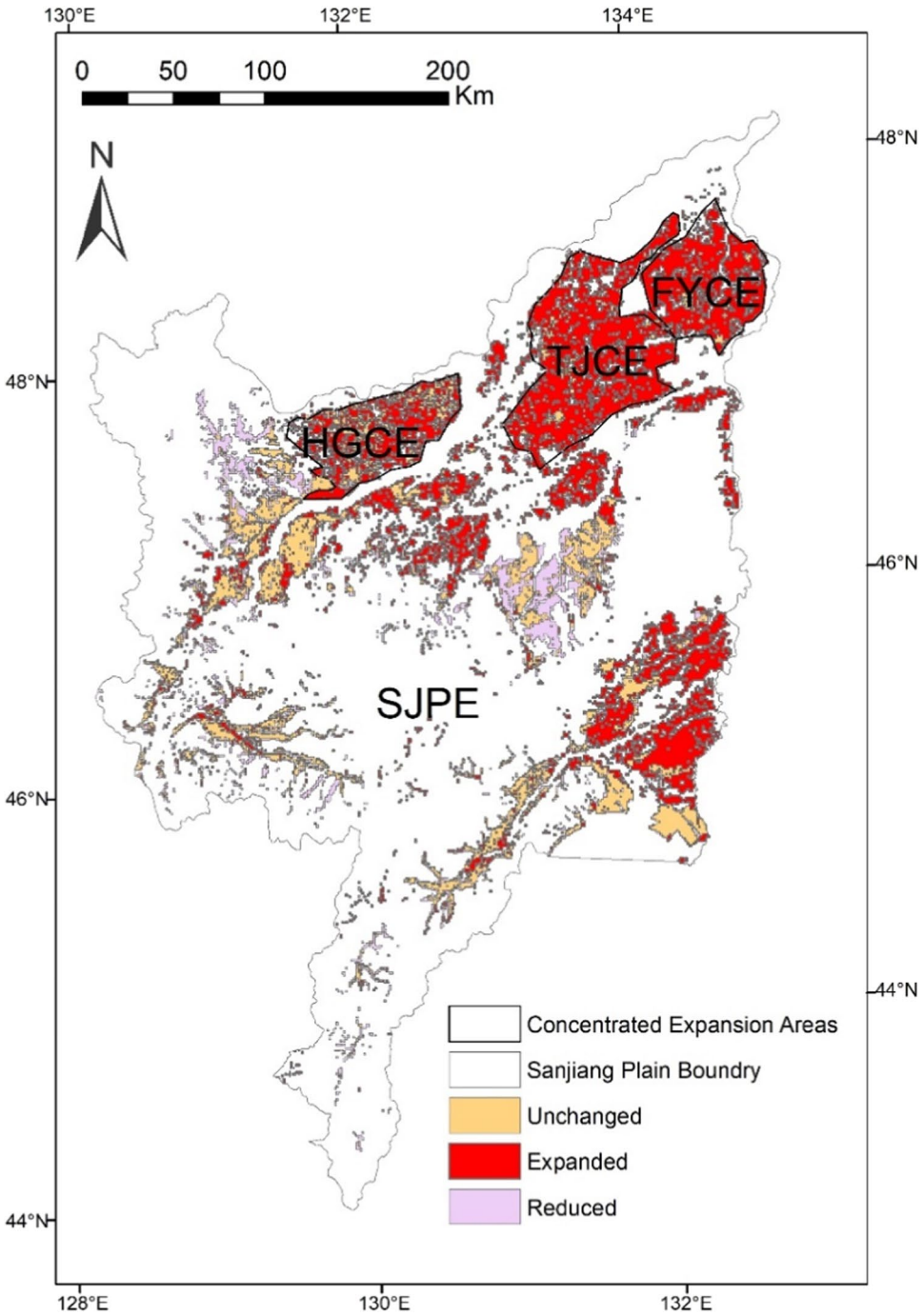

Fig. 2 Paddy areas change from 2000 to 2018 in the Sanjiang Plain

accounted for 13.2%, 16.9%, and 32.4% of Sanjiang Plain expansion zones (SJPE), respectively. TJCE was the combination of Fujin and Tongjiang counties concentrated expansion zones, which accounted for the largest ratio. HGCE and TYCE were based on the Hegang city and Fuyuan county concentrated expansion zones, respectively.

2.2 Model description

2.2.1 WRF model

Weather Research and Forecasting (WRF) model is widely used in regional climate modeling and numerical weather predictions, which is designed as a flexible and advanced atmospheric simulation system (Skamarock and Klemp 2008). The WRF model consists of WPS (WRF Pre-processing System) and ARW (Advanced Research WRF). WPS is used primarily for real-data simulations, and its functions includes defining simulation domains, interpolating terrestrial data to the simulation domain. ARW is a critical component, which is composed of several initialization programs for idealized, and real-data simulations, and the numerical integration program. The WRF version 4.2 is used in the study.

2.2.2 Parameterization schemes

The primary physical parameterization schemes involved are cloud microphysical parameterization scheme, cumulus convection parameterization scheme, planetary boundary layer scheme, land surface model, and radiation scheme. Different physical parameterization schemes of WRF model achieve different simulation results (Knievel et al. 2004; Chambon et al. 2014). The physical parameterization schemes are shown in Table 1. In this study, the Grell-Devenyi scheme for cumulus parameterization (Grell and Devenyi 2002), the Yonsei University planetary boundary layer scheme for planetary boundary layer process (Hong et al. 2006), the WRF single-moment three-class scheme for micro-physics (Hong et al. 2004), the CAM3 scheme for longwave radiation and shortwave radiation (Collins 2004), and the Noah Land Surface Model for Land Surface process (Chen and Dudhia 2001) were chosen.

2.2.3 Experiment design detail

The effects of paddy expansion on regional climate were achieved in one-way double nesting domains (Fig. 3). The outer domain was resolved with 25 km grid spacing (111×121 grids), and the inner domain was nested with 5 km grid spacing (40×40 grids) that covering the Sanjiang Plain. Input land use data of two cases for the inner domain is shown in Fig. 4. We selected the National Centers for Environmental Prediction (NCEP) Final Analysis (FNL) 1 degree resolution and 6 hourly temporal sampling data to provide the initial and boundary conditions for the WRF model simulations. The Lambert projection is used in the mid-latitude regions owing to its better applicability. The simulation period spanned from May 1, 2018, to September 30, 2018, with the first month as a spin-up to avoid an imbalance between external forcing and internal dynamics.

Paddy expansion is demonstrated by extracting the area and distribution of paddy fields, which is essentially a change in land use. The green vegetation fraction (GVF) and albedo (ALB) are two key bio-geophysical parameters that affect regional climate. The GVF has an influence on vegetation transpiration and CO_2 exchange of the vegetation canopy, and ALB affects radiation balance by absorbing shortwave. Temporally and spatially continuous GVF and ALB data manifest the connections between the land surface and atmosphere, and thus help simulate accurate impacts triggered by paddy expansion.

Irrigation cannot be ignored that it is considered a unique agricultural management measure for paddy compared to other land covers. Therefore, two numerical experiments (case A and case B) were conducted when physics parameterization option and the driving data were consistent, and land use, ALB, and GVF were modified, irrigation module was opened but irrigated land percentage have difference (Table 2).

The land use data of 2000 and 2018 were derived from the Data Center for Resources and Environmental Sciences, Chinese Academy of Sciences (http://www.resdc.

Table 1 WRF model physical parameterization schemes

Physical parameterizations	Schemes used in the experiments	Parameter specific values
Microphysics scheme	WRF Single-Moment 3-class scheme	mp_physics = 3
Longwave radiation	CAM scheme	ra_lw_physics = 3
Shortwave radiation	CAM scheme	ra_sw_physics = 3
Cumulus Parameterization	Grell–Devenyi ensemble convective	cu_physics = 3
Planetary Boundary layer	Yonsei University scheme	bl_pbl_physics = 1
Land Surface	Noah Land Surface Model	sf_surface_physics = 2

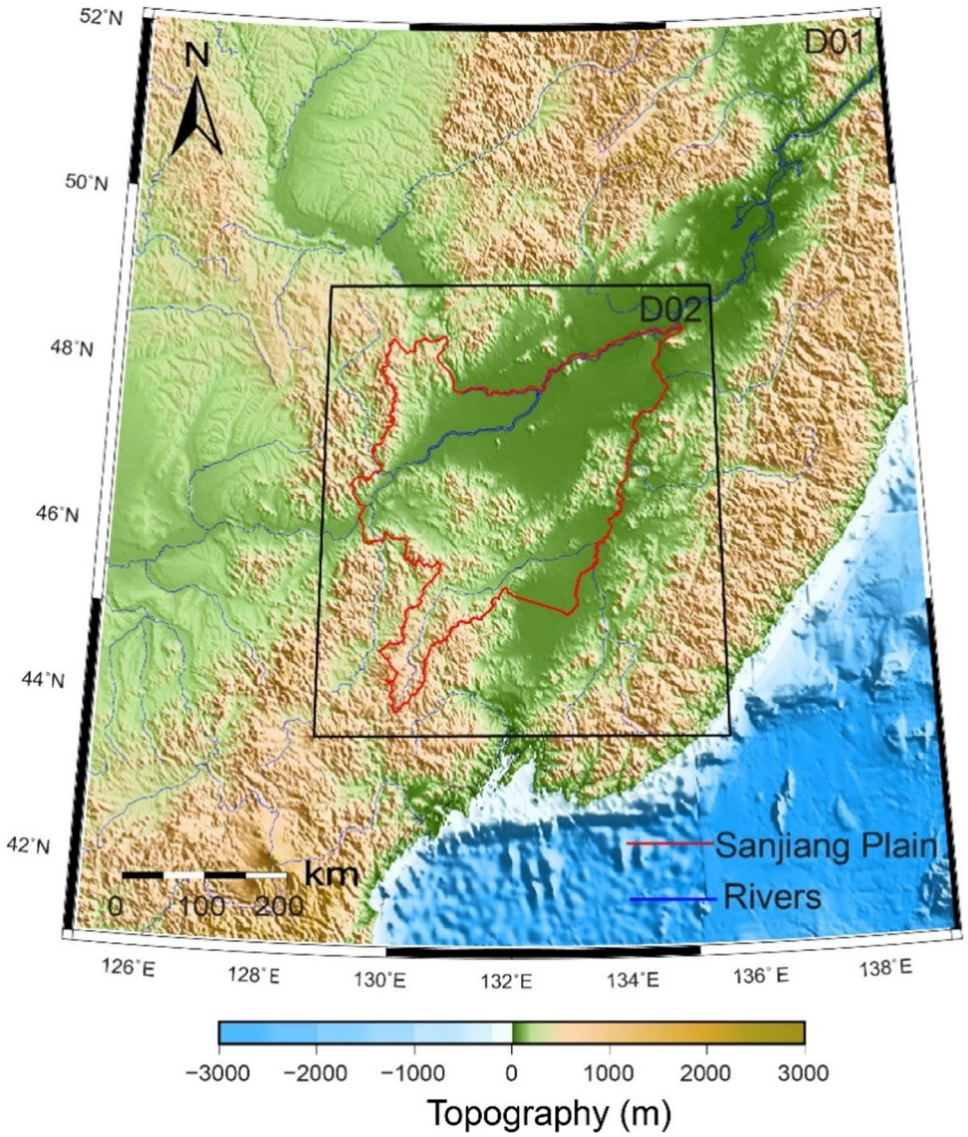

Fig. 3 The nested domain setup

cn). To accurately simulate the influence triggered merely by paddy expansion, land use data by paddy field in 2018 were extracted by attributes and then mosaic to new raster with 2000 land use data (Fig. 5), which guaranteed that the distribution of the remaining land use types except for paddy field are identical in case A and case B. For case B, the 3-year (2016–2018) simulation uniformly used the 2018 land use data, that is to say, the paddy field distribution in the three years is unchanged, and we updated the model geographical static data with ALB and GVF, which were accessed from the Global Land Surface Satellite (GLASS) dataset (http://gre.geodata.cn/thematicView/GLASS.html). However, model default geographical static data represent the spatial heterogeneity of GVF and ALB in Case A.

There are two types of land use cover data in static geographical data, which are based on USGS and MODIS. The USGS land cover data are 24 types with a spatial resolution of 30" provided by the United States Geological Survey, which are mainly obtained by processing the advanced very high-resolution radiometer (AVHRR) remote sensing data in 1992 and 1993. Table 4 is the USGS-24 land cover classification system. The two important steps of modifying the land use data read by the WRF model are shown in Figs. 5 and 6. The first is processed data so that it becomes readable by the WRF model, including the data reprojected by World Geodetic System and resampled to 30 s resolution, reclassified according to USGS-24 class standard, and output into ASCII format in ArcGIS. Then made WRF model read and apply the ASCII file in WPS module. Using Gcc and Gfortran compiles an a.out file, execute a.out file to obtain the binary file under WPS_geogrid_src directory. Add an INDEX file to the binary file under WPS_GEOG directory and modify the GEOGRIB.TBL file including rel_path and interp_option method information under WPS_geogrid

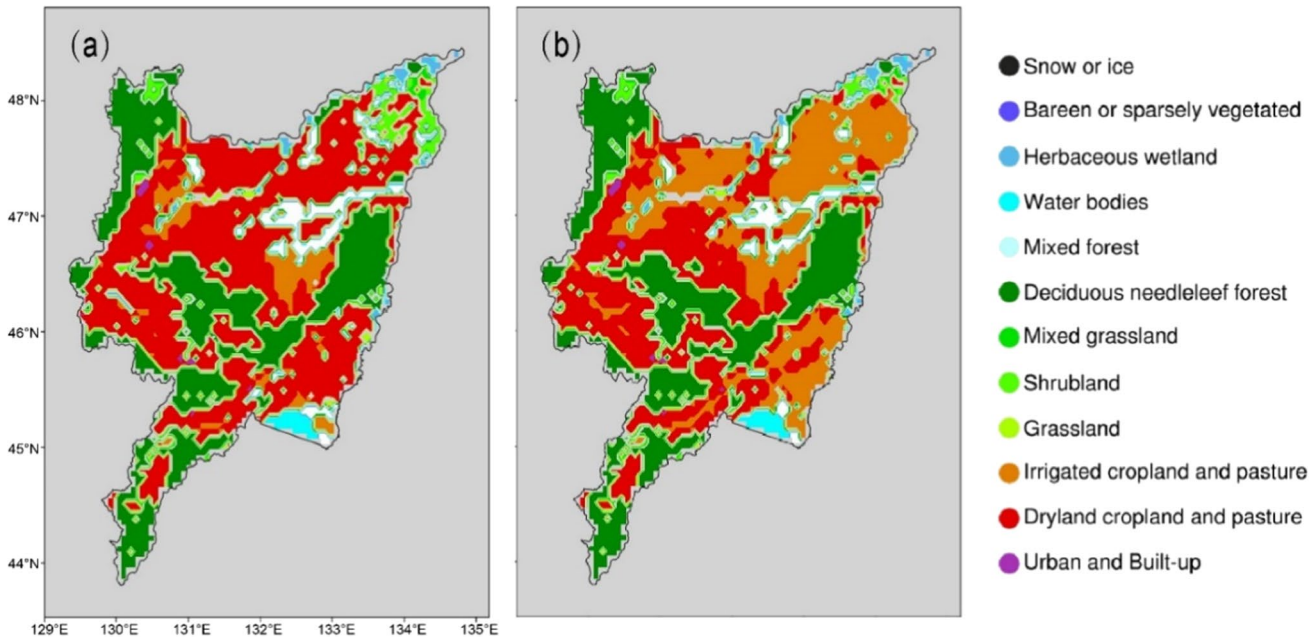

Fig. 4 WRF model input the land use map of the inner domain: **a** case A and **b** case B according to USGS-24 category

Table 2 Two numerical experiments details

i	Case A_i	Case B_i	B-A
1	Land use: 2000; FNL: 2016; GVF and ALB: WRF default; Irrigation	Land use: 2018; FNL: 2016; GVF and ALB: 2016; Irrigation	B_1-A_1
2	Land use: 2000; FNL: 2017; GVF and ALB: WRF default; Irrigation	Land use: 2018; FNL: 2017; GVF and ALB: 2017; Irrigation	B_2-A_2
3	Land use: 2000; FNL: 2018; GVF and ALB: WRF default; Irrigation	Land use: 2018; FNL: 2018; GVF and ALB: 2018; Irrigation	B_3-A_3

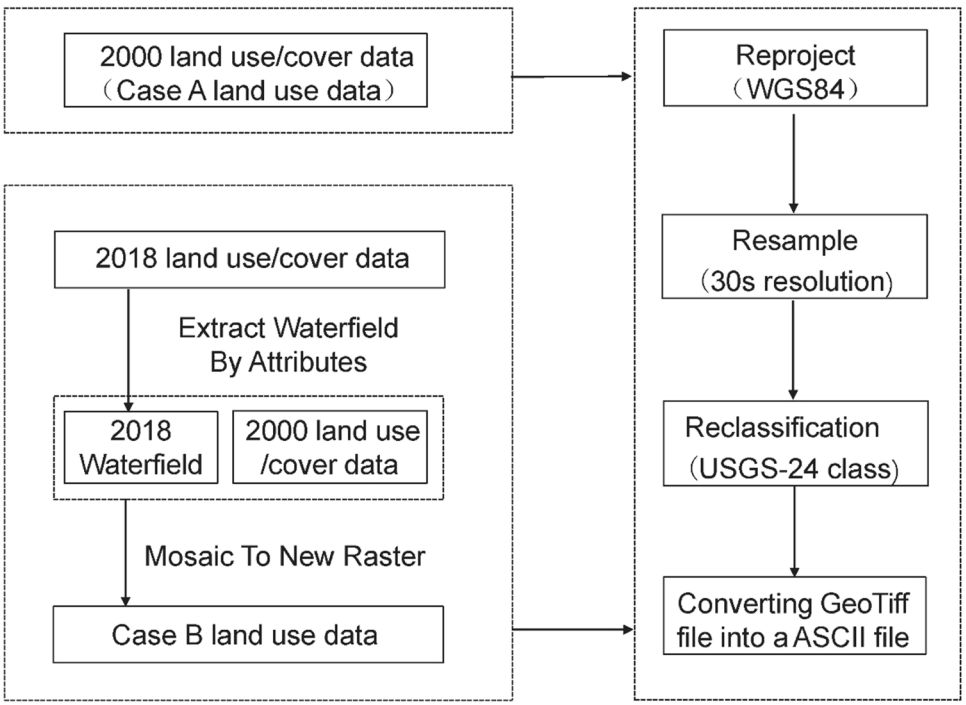

Fig. 5 Land use data production process for two cases in ArcGIS

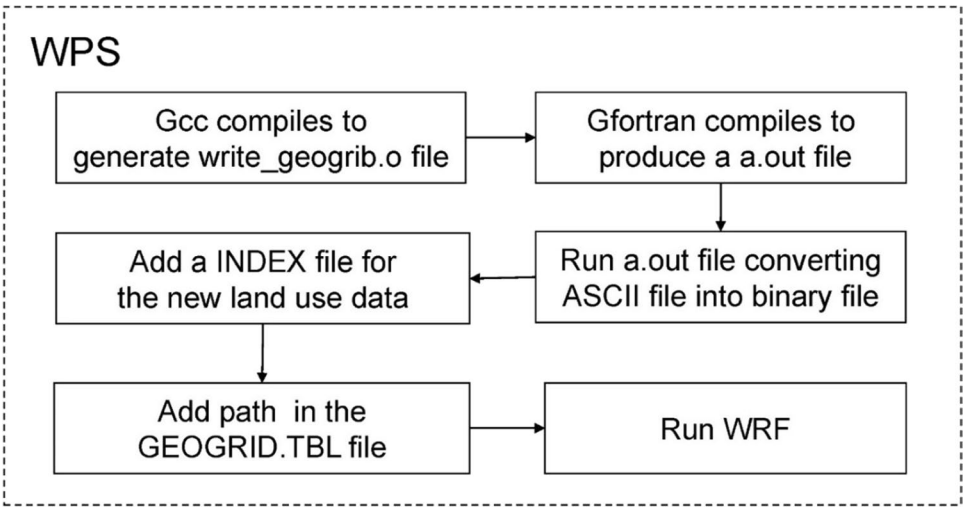

Fig. 6 The process of replacing WPS readable land use data

Table 3 Irrigation module parameter in two numerical experiments

Irrigation parameterizations	Parameter specific values
sf_surf_irr_scheme	1
irr_daily_amount	4.5
irr_start_hour	14
irr_num_hours	4
irr_start_julianday	147
irr_end_julianday	211
irr_ph	0
irr_freq	7

directory. When the above steps are completed, the normal procedure of the WRF model is followed next.

Irrigation caused by paddy expansion was also worthy of attention, which was the major difference between paddy fields and rainfed farmland. In order to quantify the impact of irrigation, case A and case B open irrigation module, while irrigated land percentage have difference. The specific irrigation parameter and irrigated land percentage are shown in Table 3 and Fig. 7, irr_daily_amount refers to previous research results about irrigation simulation in China (Liu et al. 2021b), and other parameters are consistent with the local field irrigation schedule. The irrigated land percentage of case A is WRF model Static Data for Specific Applications, which derived from WRF Static Data Downloads. And the irrigated land percentage of case B was obtained by analyzing the land use data of 2018, we consider only paddy fields required irrigation and the proportion of paddy fields area was taken as the irrigated land percentage. The major steps included divided the grid, and calculated the ratio of paddy field area within the grid to the total grid in ArcGIS, then converted into Geogrid binary format read by WPS. The different simulation results from the two cases were illustrated the impacts of paddy expansion. Considering the paddy growth period is June to September, the different months simulations results were subsequently analyzed, including June, July, August, and September, respectively (Table 4).

2.3 Evaluation index

To verify the WRF model performance, the daily temperature observation and the WRF simulation in the Sanjiang Plain was used to evaluate, the daily temperature observation was obtained from the dataset of daily near-surface air temperature in China from 1979 to 2018, which was provided by National Tibetan Plateau Data Center (http://data.tpdc.ac.cn). We chose percentage bias (PB), root mean square error (RMSE), and pattern correlation coefficient (PCC) to analyze the discrepancy between the observation and simulated data. The PB, RMSE, and PCC were calculated according to the formula as follows:

$$PB = \frac{|OBS - SIM|}{OBS} \times 100\% \quad (1)$$

where PB is the percentage bias, %; SIM is the WRF model simulated value; OBS is the meteorological station observation value.

$$RMSE = \sqrt{\frac{1}{m}\sum_{i=1}^{m}(Si - Oi)^2} \quad (2)$$

where, RMSE is root mean square error, °C; S_i and O_i are the WRF simulation values and meteorological station observation value on day i, respectively.

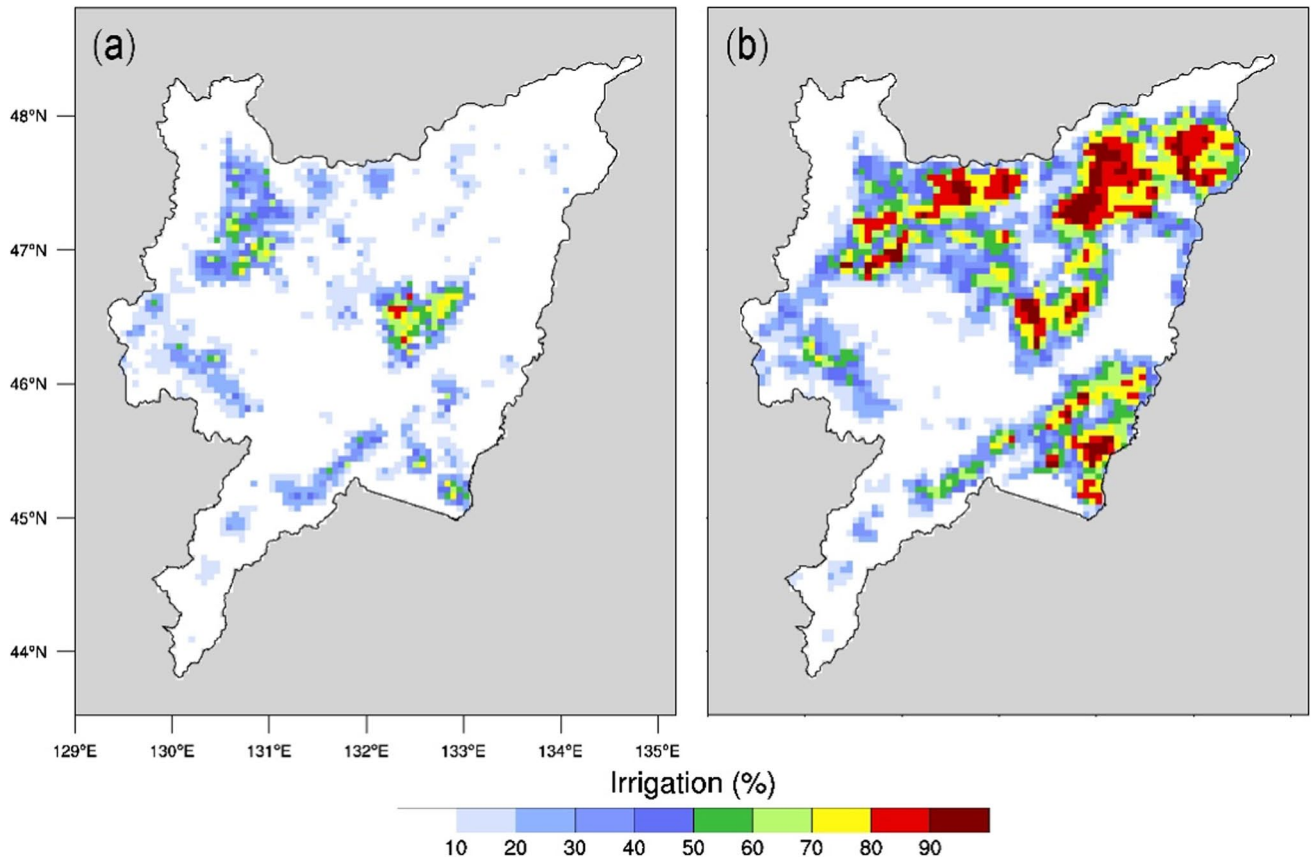

Fig. 7 Irrigated land percentage (%) in Sanjiang Plain: **a** case A, **b** case B

Table 4 USGS-24 land cover classification system in WRF model

Code	Land cover type	Code	Land cover type
1	Urban and built-up land	13	Evergreen broadleaf forest
2	Dryland cropland and pasture	14	Evergreen needleleaf forest
3	Irrigated cropland and pasture	15	Mixed forest
4	Mixed dryland/irrigated cropland and pasture	16	Water bodies
5	Cropland/grassland mosaic	17	Herbaceous wetland
6	Cropland/woodland mosaic	18	Wooded wetland
7	Grassland	19	Barren or sparsely vegetated
8	Shrubland	20	Herbaceous tundra
9	Mixed shrubland/grassland	21	Wooded tundra
10	Savanna	22	Mixed tundra
11	Deciduous broadleaf forest	23	Bare ground tundra
12	Deciduous needleleaf forest	24	Snow or ice

$$PCC = \frac{\sum_{i=1}^{n}\left(X_i - \overline{X}\right)\left(Y_i - \overline{Y}\right)}{\sqrt{\sum_{i=1}^{n}\left(X_i - \overline{X}\right)^2 \sum_{i=1}^{n}\left(Y_i - \overline{Y}\right)^2}} \quad (3)$$

where PCC is pattern correlation coefficient; X_i and Y_i are the WRF simulation values and the dataset of daily near-surface air temperature value on month i, respectively. $\overline{X}$ and $\overline{Y}$ are its mean value, respectively.

3 Results

3.1 Model validation

The WRF model performance was evaluated by comparing the simulation results with the grid observations at the grid interval of 0.5°. The RMSE, PB, and PCC of the daily temperature in the four zones are shown in Table 5, which are 2.10 °C, 6.8%, and 0.88, respectively in SJPE. The calculated values of RMSE, PB, and PCC of three concentrated expansion zones ranged from 2.32 to 2.50 °C, 7.0 to 7.8%,

Table 5 The RMSE, PB and PCC between the daily temperature simulations and observations in four zones

Expansion zones	RMSE (°C)	PB (%)	PCC
HGCE	2.32	7.2	0.85
FYCE	2.50	7.8	0.81
TJCE	2.38	7.0	0.84
SJPE	2.12	6.8	0.88

Table 6 Area of land use categories converted to paddy fields from 2000 to 2018 in four expansion zones (km^2)

	HGCE	FYCE	TJCE	SJPE
Dryland to paddy filed	1957.05	903.04	3905.28	8893.61
Woodland to paddy filed	-	1205.71	505.68	3203.79
Wetland to paddy filed	-	460.29	515.68	933.9
Grassland to paddy filed	31.63	-	-	2018.1
Water to paddy filed	13.78	-	-	148.44
Total expansion	2002.46	2569.04	4926.64	15,197.84

and 0.81 to 0.85, respectively. The results showed that (1) spatial differences were existed in the simulation performance, possibly due to surface heterogeneity which affect the WRF model simulation performance., and (2) simulation accuracy was overall better. The evaluation index values manifested a similar accuracy compared to recent research, PB and RMSE were 7.04%, 2.40 °C, respectively (Su et al. 2021), RMSE ranged from 1.64 to 2.07 °C and PCC ranged from 0.88 to 0.92 (Li et al. 2020). Therefore, it indicated that the WRF model and parameterization scheme selected in the study simulated the actual temperature process in the Sanjiang Plain.

3.2 Conversion sources for paddy expansion

To determine the conversion sources of paddy expansion in different expansion zones, we counted the areas of multiple land use types converted to paddy fields (Table 6). Paddy expansion areas were 2002.46 km^2 (HGCE), 2569.04 km^2 (FYCE), 4926.64 km^2 (TJCE), and 15,197.84 km^2 (SJPE). The three zones (HGCE, FYCE, TJCE) accounted for 13.2%, 16.9%, and 32.4% of the SJPE, respectively. Almost all of paddy expansion came from the dryland to the paddy field in HGCE, whereas, dryland, woodland, and wetland are the three main paddy land conversion types for FYCE, accounting for 35.1%, 47.0%, and 17.9% of the total FYCE, respectively. Dryland is the most dominant type of paddy fields conversion with a proportion of 79.2, wetland and woodland conversion areas were close to in TJCE. For SJPE paddy converted area, dryland, woodland, grassland, wetland, and water accounted for 58.5%, 21.1%, 13.3%, 6.1%, and 1.0%, respectively.

3.3 Surface parameter value adjustment

Previous numerical simulations studies revealed that vegetation parameters including surface albedo, green vegetation fraction, and leaf area index were sensitive to simulation results (Myhre and Myhre 2003; Vahmani and Hogue 2014; Alexandru and Sushama 2016; Yan et al. 2019). Improved and refined WRF model simulation required high precision data (Yu et.al. 2019). Given that the study is more concerned with the impacts of land cover change, only the vegetation parameters related to land cover are adjusted.

The two experimental differences of averaged ALB from June to September are shown in Table 7. The results demonstrated that ALB consistently increased from June to September in HGCE and TJCE, and ranged from 0.016 to 0.025 and 0.0058 to 0.0134, respectively. However, the opposite trend was observed in the ALB of SJPE with a slight reduction, and a remarkable reduction in the average ALB of FYCE that ranged from 0.028 to 0.031. The regional differences of ALB caused by paddy expansion were emerged in different regions, with an increase and a decrease. Meanwhile, monthly analysis indicated most increased in August and September for HGCE and TJCE, with maximum reduction for FYCE in June, a slight reduction from June to July and the opposite trend was demonstrated with a slight increase in August and September for SJPE. The change of ALB was closely related to multiple factors, including irrigation, vegetation growth, and crop species. For FYCE, where indicated that extensive irrigated paddy field reduce albedo due to the most exposed water surface in June compared to other three months of study (Liu et al. 2019). The GVF trend also manifested a significant increase in four expansion zones (Table 7). The highest increase in GVF (20.38%)

Table 7 The difference of ALB and GVF between case A and case B from June to September

Expansion zones	ALB				GVF			
	June	July	August	September	June	July	August	September
HGCE	0.015	0.019	0.025	0.025	0.06	9.45	7.63	1.96
FYCE	−0.029	−0.031	−0.029	−0.028	0.50	6.77	6.83	4.00
TJCE	0.0059	0.0086	0.0127	0.0134	3.78	8.41	6.00	2.20
SJPE	−0.0010	−0.0002	−0.0008	−0.0005	1.59	5.55	5.97	4.54

was recorded for TJCE, followed by HGCE (18.98%), SJPE (17.66%), and FYCE (17.12%), respectively. From a monthly perspective, July and August saw the largest increase in all expansion zones, whereas expansion was the lowest in June for FYCE and SJPE, and the same was the lowest in September for HGCE and TJCE. Overall, GVF showed a significant increase with paddy expansion, especially in July, and the magnitude of increase is related to previously grown crops at local scale.

3.4 Impacts of paddy expansion on near-surface temperature

The potential effects of paddy expansion on near-surface temperature were illustrated by the spatial variation distribution (Fig. 8). The near-surface temperature response to paddy expansion was significantly different in different zones and the cumulative growth period temperature ranged from − 0.43 °C in SJPE (the lowest) to − 0.80 °C HGCE

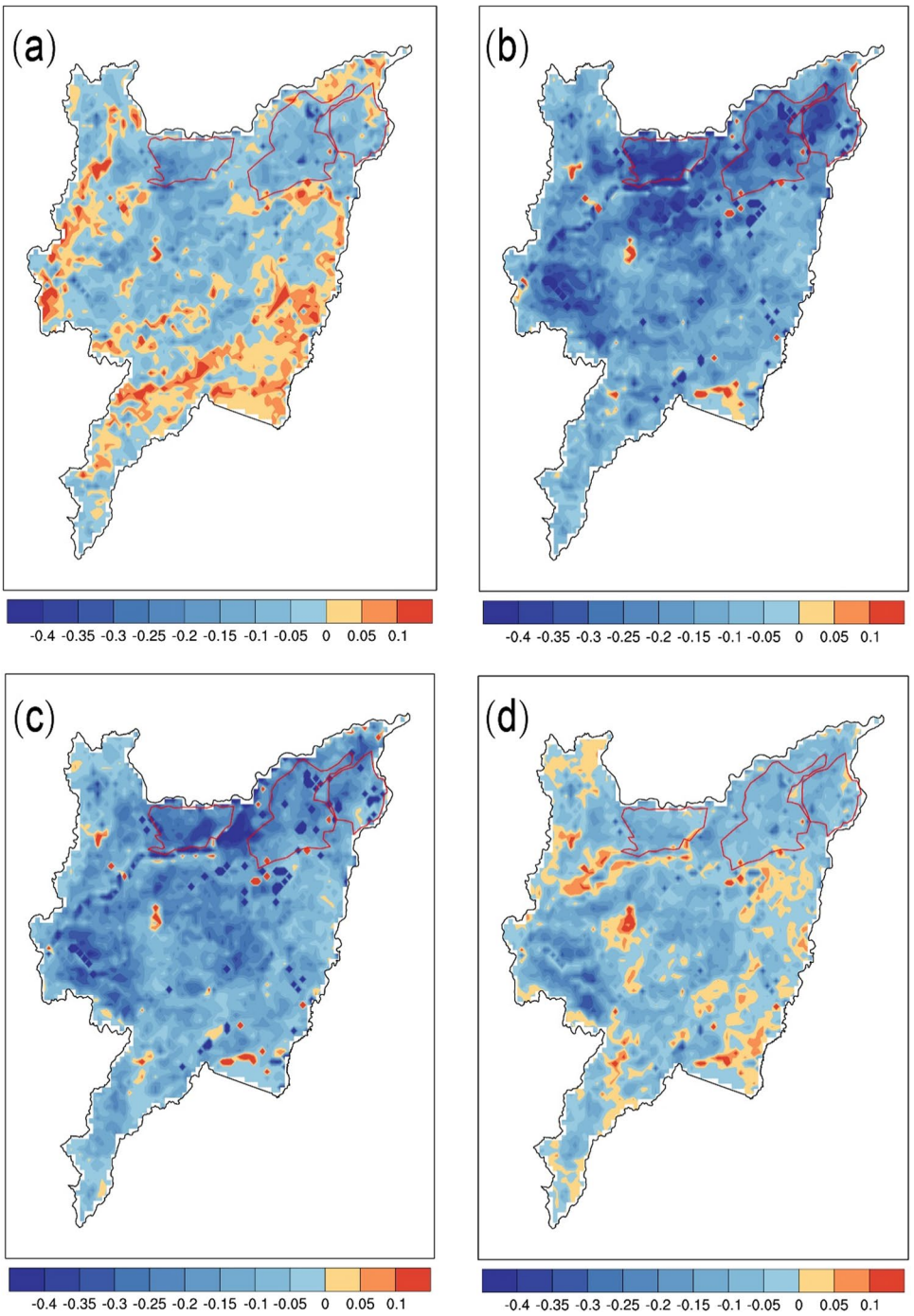

Fig. 8 Differences in simulated T (°C) between case A and case B: **a** June, **b** July, **c** August, and **d** September

(the highest). The cooling effect in SJPE was the lowest compared with other three concentrated expansion zones (HGCE, TJCE, FYCE), indicating that the local scale has more significant cooling effect than the plain scale. It was only the surface explanation that spatial heterogeneity for the three concentrated expansion regions were located at higher latitudes compared to the Sanjiang Plain. Another contributing factor was that the three concentrated expansion zones were merely paddy expansion, while various land use transitions were intertwined, some land use changes have opposite effects on paddy expansion, which further counteracted the impact of paddy expansion in the Sanjiang Plain. The relationship between the expansion ratio and temperature decrease was deserved to be focused on. As a result, we concluded that the cooling effect reflects regional heterogeneity, which has no linear relationship with expansion areas but related to what kinds of land use was converted to paddy fields. On monthly basis, paddy area expansion has little effect on temperature drop in July as against August where more visible drop in temperature was recorded with paddy area expansion (Table 8). On average, temperature decrease was the largest in July and August (0.238 °C) for four expansion zones, while decreases by an average of merely 0.077 °C in June and September. The results showed that the cooling effect has significant monthly variability and the paddy fields encountered the largest temperature drop in July and August due to greatest GVF change.

Radiative and non-radiative processes contributed to the temperature changes of paddy expansion, the warming effect of radiative processes due to a lower ALB absorbs more solar radiation, and the cooling effect of non-radiative processes was caused by GVF increase, which promotes evaporation. From June to September, the ALB showed a significant change with a cumulative increase of 0.086 in HGCE and 0.04 in TJCE, and a decrease of 0.118 in FYCE, whereas, GVF increased significantly in three concentrated expansion zones. However, the cumulative temperature decrease is almost constant in three concentrated expansion zones, which suggested that the radiative process triggered by changing ALB has a weaker effect on temperature, and it is evapotranspiration that initiates the dominant effect.

Table 8 The expansion ratio and simulated temperature differences in four zones from June to September

Expansion zones	Expansion ratio (%)	Temperature (°C)			
		June	July	August	September
HGCE	10.69	−0.121	−0.335	−0.263	−0.082
FYCE	13.23	−0.068	−0.265	−0.195	−0.080
TJCE	25.49	−0.098	−0.283	−0.226	−0.078
SJPE	100	−0.034	−0.179	−0.155	−0.058

3.5 Impacts of paddy expansion on energy budget

Paddy expansion affects energy balance and partitioning in terms of analyzing energy flux change between case A and case B. The changes in latent heat flux (LH), sensible heat flux (SH), and ground heat flux (G) from June to September are shown in Figs. 9, 10, and 11, respectively. During the whole growing seasons, the LH in the FYCE demonstrated the highest total increase at 55.29 Wm^{-2} due to the largest decrease in albedo, indicating that paddy expansion increased LH by decreasing ALB. The LH increase in TJCE was 13.49 Wm^{-2}, and 6.18 Wm^{-2} in HGCE, which manifested that albedo increase has a weak influence on LH increase. The SH decreased by 19.43 Wm^{-2}, 19.97 Wm^{-2}, and 14.31 Wm^{-2} in HGCE, FYCE, and TJCE, respectively. Meanwhile, the trend of G change was consistent with the abovementioned trend of LH and SH change, and its highest growth value was recorded in the FYCE, which ranged from 1.22 to 2.70 Wm^{-2}. For the three concentrated expansion zones, we found that ALB and GVF influenced energy balance; GVF increase caused a decrease in SH decreased and an increase in LH and G. Among the four zones, the largest changes in LH, SH, and G occurred in FYCE, which was mainly induced by ALB.

There were substantial monthly variations in terms of surface energy (Figs. 9, 10, and 11). Three concentrated expansion zones were analyzed together, where LH was increased by 19.03 Wm^{-2}, 31.03 Wm^{-2}, 19.18 Wm^{-2}, and 5.73 Wm^{-2} in June, July, and August, and September respectively. The SH was reduced by 11.26 Wm^{-2}, 20.67 Wm^{-2}, 15.74 Wm^{-2}, and 6.05 Wm^{-2} in June, July, August, and September, respectively. The most significant energy changes appeared in July and August. Considering the GVF increase reached a peak and ALB almost unchanged, paddy evapotranspiration played a dominant role in July. Both ALB increase and GVF increase enhanced sensible heat convert to latent heat, which caused the energy transformation in August. As expected, a significant monthly variation was also observed in G, while the change in G was relatively small compared to LH and SH. The G decreased by 1.18 Wm^{-2} in September, and increased by 3.36 Wm^{-2}, 3.82 Wm^{-2}, and 0.37 Wm^{-2} in June, July, and August, respectively. It demonstrated that paddy expansion increased G in June, July, and August, while decreased it in September.

4 Discussion

The effect of LUCC on surface energy distribution and temperature mainly depends on the changes of land surface biophysical parameters (Cao et al. 2015). During the paddy expansion, land use types and irrigation affects biophysical parameters of land surface. In this study, we not only

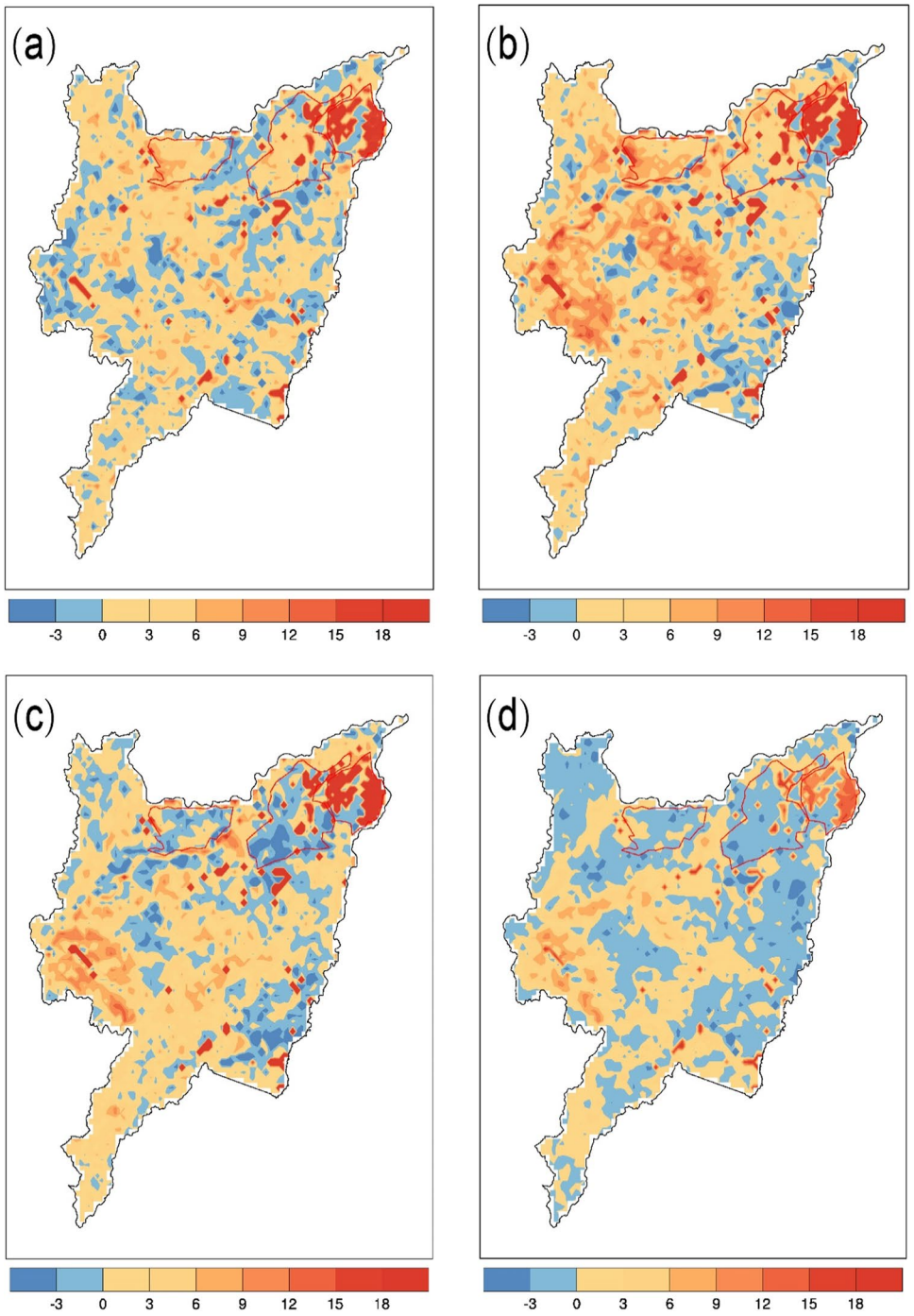

Fig. 9 Differences in Simulated LH (W m^{-2}) between case A and case B: **a** June, **b** July, **c** August, and **d** September

used the WRF model that has a high-resolution and physical process perfection, but also incorporated with multiple remote sensing-based vegetation indexes (GVF and ALB) to simulate climate impacts response on paddy expansion accurately in Sanjiang Plain. Meanwhile, the differential impacts triggered by different expansion zones and months were analyzed considering conversion sources (Table 6).

4.1 Impacts of paddy expansion on temperature

In the context of global warming, the surface temperature was widely studied by numerous climate models because of the critical role of surface temperature in controlling crop evapotranspiration and attribution of measuring energy balance (Shi et al. 2007; Jin and Dickinson 2010; Du et al. 2019;

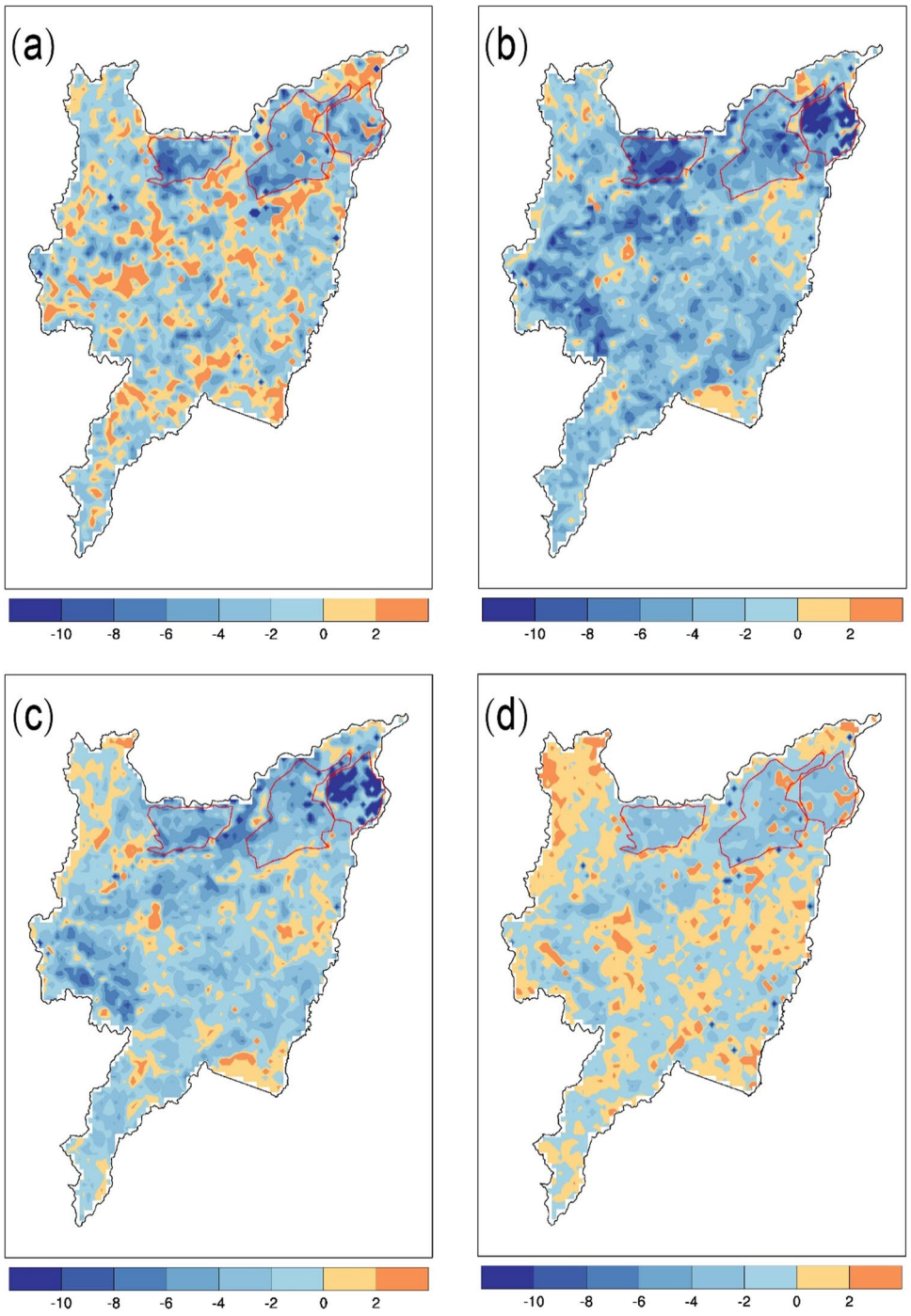

Fig. 10 Differences in simulated SH (W m^{-2}) between case A and case B: **a** June, **b** July, **c** August, and **d** September

Li et al. 2020; Yu et al. 2020; Su et al. 2021). During the growing seasons, we found a decreasing trend with different intensities in surface temperature regardless of location. The effect of paddy expansion was accurately simulated using WRF model compared to merely analyzing remote sensing data, which excluded the climate warming and inter-annual differences. Previous studies have analyzed the impact of paddy expansion using remote sensing data in the Sanjiang plain and noted a significant near-surface cooling in spring (May and June) rather than summer (July and August) and autumn (September) (Liu et al. 2018). The land surface temperature decrease ranged from 0.6 to 5.1 °C between the high and low levels from May to October (Du et al. 2019). Recent studies have concentrated on simulating temperature changes based on the WRF model (Yu et al. 2020; Li et al. 2020; Zheng et al. 2020; Su et al. 2021). Paddy expansion had a greater impact on temperature than urbanization, and vegetation greening. Su et al. (2021) found that urban

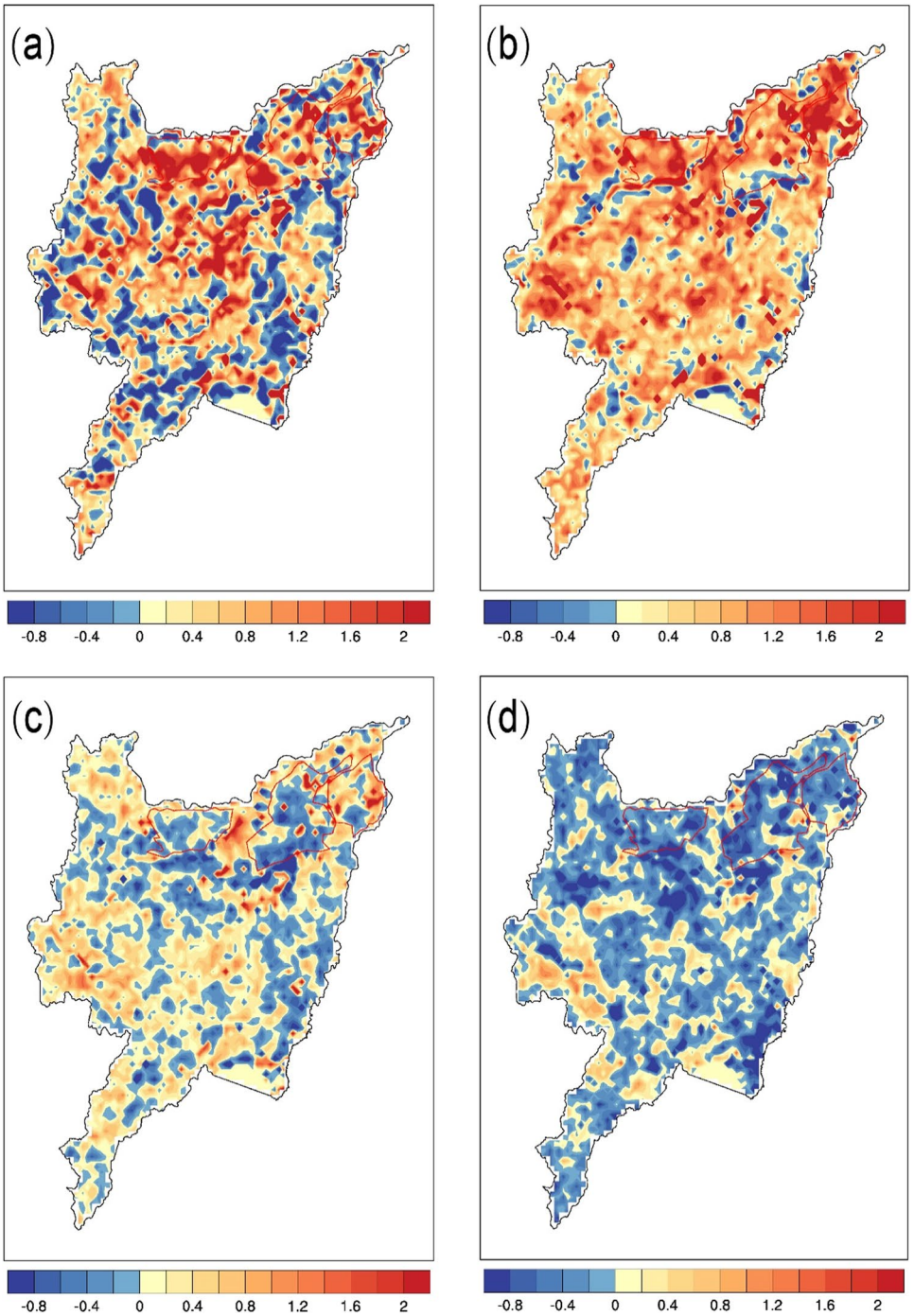

Fig. 11 Differences in simulated G (W m^{-2}) between case A and case B: **a** June, **b** July, **c** August, and **d** September

temperatures increase by 0.104 °C in 2020 compared with 1980, while Yu et al. (2020) found 0.11 °C decrease in surface temperature induced by vegetation greening.

In the process of paddy expansion, land transformation patterns determine whether radiative process or non-radiative process play a leading role by changing ground parameters (ALB, GVF). The temperature effects of paddy expansion are closely related to land transformation patterns, which are embodied in warming up to 1.31 °C from wetland to dryland, however, a cooling effect of 1.32 °C is caused by dryland convert to paddy fields (Liu et al. 2018). Conversions from forest to cropland have a warming impact on local temperature (0.03 °C/decade) due to decreased latent heat (Jin et al. 2021). The conversion sources (Table 6) contributed to analyzing the non-linearly relationship between the paddy expansion ratio and temperature decline (Hu et al. 2021). The lowest temperature drop in FYCE may be due to the conversion of a high percentage of woodland to paddy

field, and the cooling impact of woodland to paddy field is weaker than that of dryland to paddy field. Meanwhile, the cooling impact triggered by paddy expansion was intimately connected with the location and irrigation (Lobell et al. 2009; Sorooshian et al. 2011; Selman and Misra 2016; Li et al. 2020).

In our results, the greatest surface temperature differences appeared in July and August, which was consistent with Kueppers et al. (2007). The paddy irrigation time was June to mid-August, more irrigation was applied in these months increased soil moisture, accelerated evaporation, and ultimately led to decrease temperature. Although the major difference between paddy fields and rainfed farmland is irrigation, temperatures drop more in September than in June, which indicated that the effect of irrigation was limited. And the essence of paddy expansion was land use change, which was the decisive factor in determining the temperature reduction. The present findings are against with Liu et al. (2019) who observed more surface cooling in May and June which was induced by excessive irrigation. However, our results validated the inferences that the significant surface temperature response may continue into July and August if paddy field expansion occurs in a dry year or region (Liu et al. 2019).

4.2 Impacts of paddy expansion on energy budget

The surface energy analysis is of great help to understand the dominant bio-geophysical mechanism driving climate change (Yu et al. 2020). The non-radiative processes dominate both the bio-geophysical effects caused by wetland reclamation and paddy field expansion, indicating that energy redistribution of latent heat and sensible heat is the chief path to transfer regional climates for land use changes (Liu et al. 2018). Paddy expansion is not just concerning land use changes, especially irrigation due to the water requirements of paddy but also affect the distribution of surface energy by altering the land surface physical properties (Pielke et al. 2002). The surface energy fluxes are inevitably redistributed due to land use conversions (Li et al. 2020). Irrigation increases LH by increasing soil evaporation and crop transpiration. And the irrigation-induced increases in LH led to the decrease of the surface energy allocated to SH (Wu et al. 2018). Irrigation causes water evaporation to remove a large amount of heat in the form of LH, and LH release also mainly depends on vegetation transpiration, which explained that energy flux changes due to paddy expansion.

Agricultural expansion redistributed surface energy fluxes, which has been convinced by past studies (Sampaio et al. 2007; Jiang et al. 2014). Our results also showed that paddy expansion changes surface energy fluxes. During the growing seasons, we found that LH increase cumulatively by 6.18–55.30 Wm^{-2}, SH decrease by 6.92–19.97 Wm^{-2}, and G increase ranged from 1.22 to 2.70 Wm^{-2} in four expansion zones. The trends of energy fluxes were consistent with Jiang et al. (2014), which stated that LH increase by 12.10 Wm^{-2}, and SH decrease by 8.85 Wm^{-2} which was mainly induced irrigated agriculture. However, opposite trend was observed by Gilvan et al. (2007) where both pasture and soybean cropland expansion increased SH and decreased LH. These findings support the trends observed in the present study and suggests that the trend of energy fluxes was related to the agricultural expansion type.

The energy flux changes had seasonal variation, with largest changes in July, followed by August. Similar results were found that the difference of *f* values (Δf) for paddy fields were the highest in July and then in August, which suggested that irrigation contributed to the shift from LH to SH in mid-summer (June and July), whereas vegetation transpiration has become the dominant factor affecting LH in late summer (Liu et al. 2018). In this study, the paddy expansion had the largest influence on LH, followed by SH, and G respectively suggesting that LH is more sensitive and G is less influenced due to paddy expansion. The present findings are in close agreement with previous model studies such as, Li et al. (2020) who found that the LH and SH considerably varied due to land conversion when anthropogenic effects were weak. While Jiang et al. (2014) found that irrigated cropland expansion made the SH change close to three-quarters of LH in summer.

4.3 Limitations and future research

Although global warming factor was excluded and the impact of paddy expansion on surface temperature and energy flux was evaluated by using the WRF model, the results provide valuable information for crop structure adjustment and agricultural irrigation. However, the design of our WRF model remains to be improved in the following. Firstly, it is indispensable to obtain high-resolution land use data to describe accurately paddy expansion distribution. Secondly, a dynamic irrigation simulation scheme is required to improve simulation reliability where dynamic irrigation accurately represent the unique agricultural management practices for paddy. In addition, the simulation effect merely selected three years for validation, more studies with varying rainfall level year, including wet, dry, and normal rainfall, are recommended for future studies to arrive at broader conclusions.

5 Conclusions

In the work, two cases were designed to simulate the effects of paddy expansion on temperature and surface energy flux with the help of the WRF model in the

Sanjiang plain. Remote sensing data (GVF and ALB) were used for adjusting WRF ground parameters in different land cover states. The following main conclusions were obtained: (1) paddy expansion significantly increased GVF ranged from 17.12 to 20.38% during the growing season, and increased or decreased ALB depended on which land use type converted to paddy field in different expansion zones. (2) Paddy expansion decreased the near-surface temperature. During the growing season, cumulative temperature declined 0.80 °C (HGCE), 0.61 °C (FYCE), 0.69 °C (TJCE), and 0.43 °C (SJPE) from June to September and much significant near-surface cooling in summer (July and August). (3) Paddy expansion affects energy balance and partitioning with a cumulative increase in LH, and a cumulative decrease in SH from June to September. (4) Paddy expansion had scale effects on temperature and energy flux. Temperature, LH and G decline as well as SH increase was significantly higher in SJPE compared with the three concentrated expansion zones (HGCE, FYCE, TJCE). (5) The changes in near surface temperature were mainly caused by evapotranspiration due to GVF increase rather than the radiative process caused by the ALB.

Acknowledgements The observed meteorological data was supported by the China Meteorological Data Sharing Service System, the Dataset of daily near-surface air temperature in China from 1979 to 2018 was provided by National Tibetan Plateau Data Center (http://data.tpdc.ac.cn), and the remote sensing data (GVF and ALB) was supported by the Global Land Surface Satellite dataset, and the land use information was provided by the Data Center for Resources and Environmental Sciences, Chinese Academy of Sciences. We also would like to thank the anonymous reviewers for their valuable comments.

Author contribution All authors contributed to the study conception and design. Peng Huang: software, methodology, writing—original draft. Dan Li: methodology, software, writing—review and editing. Hua Xie: methodology, funding acquisition. Chaoli Liu: data curation. Hayat Ullah: resources. Yang Xu: funding acquisition, data curation. Changhong Song: supervision. Chunsheng Dai: supervision. Yuanlai Cui: conceptualization, Resources. Yufeng Luo: methodology, investigation, funding acquisition, writing—review and editing. All authors have read and approved the final manuscript.

Funding This study was financially supported by the National Natural Science Foundation of China (51979201 and 51779187) and the Water Resources S&T Project of Inner Mongolia Autonomous Region, China (No. NSK 2021–01).

Data availability The China Meteorological Data Sharing Service System downloaded from http://data.cma.gov.cn, the land use information provided by the Data Center for Resources and Environmental Sciences, Chinese Academy of Sciences (http://www.resdc.cn). The Global Land Surface Satellite dataset for remote sensing data support (http://gre.geodata.cn/thematicView/GLASS.html). The dataset of daily near-surface air temperature in China from 1979 to 2018 is provided by National Tibetan Plateau Data Center (http://data.tpdc.ac.cn).

Code availability All codes related to this paper may be requested from the corresponding author.

Declarations

Ethics approval Not applicable.

Consent to participate Not applicable.

Consent for publication Not applicable.

Conflict of interest The authors declare no competing interest.

References

Alexander P, Rounsevell MDA, Dislich C, Dodson JR, Engström K, Moran D (2015) Drivers for global agricultural land use change: the nexus of diet, population, yield and bioenergy. Glob Environ Chang 35:138–147. https://doi.org/10.1016/j.gloenvcha.2015.08.011

Alexandru A, Sushama L (2016) Impact of land-use and land-cover changes on CRCM5 climate projections over North America for the twenty-first century. Clim Dyn 47(3):1197–1209. https://doi.org/10.1007/s00382-015-2896-3

Anderson FE, Snyder RL, Miller RL, Drexler J (2003) A micrometeorological investigation of a restored California wetland ecosystem. Bull Am Meteor Soc 84(9):1170–1172. https://doi.org/10.1175/BAMS-84-9-1170

Arvor D, Meirelles M, Dubreuil V, Begue A, Shimabukuro YE (2012) Analyzing the agricultural transition in Mato Grosso, Brazil, using satellite-derived indices. Appl Geogr 32:702–713. https://doi.org/10.1016/j.apgeog.2011.08.007

Bala G, Caldeira K, Wickett M, Phillips TJ, Lobell DB, Delire C, Mirin A (2007) Combined climate and carbon-cycle effects of large-scale deforestation. Proc Natl Acad Sci USA 104(16):6550–65555. https://doi.org/10.1073/pnas.0608998104

Bai M, Mo XG, Liu SX, Hu S (2019) Contributions of climate change and vegetation greening to evapotranspiration trend in a typical hilly-gully basin on the Loess Plateau, China. Sci Total Environ 657:325–339. https://doi.org/10.1016/j.scitotenv.2018.11.360

Betts RA, Falloon PD, Goldewijk KK, Ramankutty N (2007) Biogeophysical effects of land use on climate: Model simulations of radiative forcing and large-scale temperature change. Agric for Meteorol 142:216–233. https://doi.org/10.1016/j.agrformet.2006.08.021

Bonfils C, Lobell D (2007) Empirical evidence for a recent slowdown in irrigation induced cooling. P Natl Acad Sci USA 104(34):13582–13587. https://doi.org/10.1073/pnas.0700144104

Brian S (2009) Land use as climate change mitigation. Environ Sci Technol 43:9052–9056

Bright RM, Davin E, O'Halloran T, Pongratz J, Zhao K, Cescatti A (2017) Local temperature response to land cover and management change driven by non-radiative processes. Nature Climate Change 7:296–302. https://doi.org/10.1038/nclimate3250

Burakowski E, Tawfik A, Ouimette A, Lepine L, Novick K, Ollinger S, Zarzycki C, Bonan G (2018) The role of surface roughness, albedo, and Bowen ratio on ecosystem energy balance in the Eastern United States. Agric for Meteorol 249:367–376. https://doi.org/10.1016/j.agrformet.2017.11.030

Burkett V, Kusler J (2000) Climate change: potential impacts and interactions IN wetlands OF the untted states 1. JAWRA J Am Water Resour Assoc 36:313–320. https://doi.org/10.1111/j.1752-1688.2000.tb04270.x

Cao Q, Yu D, Georgescu M, Han Z, Wu J (2015) Impacts of land use and land cover change on regional climate: a case study in the

agro-pastoral transitional zone of China. Environ Res Lett 10. https://doi.org/10.1088/1748-9326/10/12/124025
Chambon P, Zhang SQ, Hou AY, Zupanski M, Cheung S (2014) Assessing the impact of pre-GPM microwave precipitation observations in the Goddard WRF ensemble data assimilation system. Q J R Meteorol Soc 140:1219–1235. https://doi.org/10.1002/qj.2215
Chen F, Dudhia J (2001) Coupling an advanced land surface-hydrology model with the Penn State-NCAR MM5 modeling system. Part I: model implementation and sensitivity. Mon Weather Rev 129(4):569–585
Chen H, Zhang WC, Gao HR, Nie N (2018) Climate Change and Anthropogenic Impacts on Wetland and Agriculture in the Songnen and Sanjiang Plain, Northeast China. Remote Sens-Basel 10(3):356. https://doi.org/10.3390/rs10030356
Collins WD, Rasch PJ, Boville BA, Hack JJ, McCaa JR, Williamson DL, Kiehl JT, Briegleb B, Bitz C, Lin S-J (2004) Description of the NCAR community atmosphere model (CAM 3.0). NCAR Tech Note NCAR/TN-464+ STR 226:1326–1334
Dan L, Ji JJ, Ma ZG (2007) The variation of net primary production and leaf area index over Xinjiang Autonomous Region and its response to climate change. Acta Ecological Sinica 27:3582–3592
Dong J, Liu X, Huang G, Fan J, Wu L, Wu J (2021) Comparison of four bio-inspired algorithms to optimize KNEA for predicting monthly reference evapotranspiration in different climate zones of China. Comput Electron Agr 186:106211. https://doi.org/10.1016/j.compag.2021.106211
Du GM, Liu WQ, Pan T, Yang HX, Wang Q (2019) Cooling effect of paddy on land surface temperature in cold China based on MODIS data: a case study in northern Sanjiang Plain. Sustainability 11(20):5672. https://doi.org/10.3390/su11205672
Erwin KL (2009) Wetlands and global climate change: the role of wetland restoration in a changing world. Wetlands Ecol Manage 17(1):71–84. https://doi.org/10.1007/s11273-008-9119-1
Feddema JJ, Oleson K, Mearns LO, Meehl GA (2005) The importance of land-cover changes in simulating future climates. Science 310:1674–1678
Gao J, Liu Y (2011) Climate warming and land use change in Heilongjiang Province, Northeast China. Appl Geogr 31(2):476–482. https://doi.org/10.1016/j.apgeog.2010.11.005
Gao S, Nie S, Liu Q (2020) Analysis of current situation of rice industry in Heilongjiang Province and Its Future Development Ideas. China Rice 26:104–106
Gibbard S, Caldeira K, Bala G, Phillips TJ, Wickett M (2005) Climate effects of global land cover change. Geophys Res Lett 32. https://doi.org/10.1029/2005GL024550
Gregory PJ, Ingram JSI, Andersson R, Betts RA, Brovkin V, Chase TN (2002) Environmental consequences of alternative practices for intensifying crop production. Agr Ecosyst Environ 88:279–290. https://doi.org/10.1016/S0167-8809(01)00263-8
Grell GA, Devenyi D (2002) A generalized approach to parameterizing convection combining ensemble and data assimilation techniques. Geophys Res Lett 29(14):1693. https://doi.org/10.1029/2002GL015311
Han S, Tang Q, Xu D, Yang Z (2018) Impacts of urbanization and agricultural development on observed changes in surface air temperature over mainland China from 1961 to 2006. Theor Appl Climatol 135(3):1595–1607. https://doi.org/10.1007/s00704-018-2461-1
Hong S-Y, Dudhia J, Chen S-H (2004) A revised approach to ice microphysical processes for the bulk parameterization of clouds and precipitation. Monthly Weather Review 132:103–120. https://doi.org/10.1175/1520-0493(2004)1322.0.CO;2
Hong S, Noh Y, Dudhia J (2006) A new vertical diffusion package with an explicit treatment of entrainment processes. Mon Weather Rev 134(9):2318–2341. https://doi.org/10.1175/MWR3199.1
Hu X, Chen M, Liu D, Li D, Jin L, Liu S (2021) Reference evapotranspiration change in Heilongjiang Province, China from 1951 to 2018: the role of climate change and rice area expansion. Agric Water Manag 253:106912. https://doi.org/10.1016/j.agwat.2021.106912
Intergovernmental Panel on Climate Change (IPCC) 2001. Impacts, adaptation, and vulnerability: contribution of Working Group II to the Third Assessment Report of the Intergovernmental Panel on Climate Change, edited by J. J. McCarthy et al. 1032. Cambridge Univ. Press, New York.
Jia Y, Cui N, Wei X, Hu X, Gong D, Feng Y (2016) Impact of climate change and irrigation on the reference crop evapotranspiration in Dujiangyan Irrigated Area. J Sichuan Univ Eng Sci Ed 1:69–79 (**(in Chinese with English abstract)**)
Jiang L, Ma E, Deng X (2014) Impacts of irrigation on the heat fluxes and near-surface temperature in an inland irrigation area of northern China. Energies (Basel) 7(3):1300–1317. https://doi.org/10.3390/en7031300
Jin M, Dickinson R (2010) Land surface skin temperature climatology: benefitting from the strengths of satellite observations. Environ Res Lett 5:044004. https://doi.org/10.1088/1748-9326/5/4/044004
Jin X, Jiang P, Du H, Chen D, Li M (2021) Response of local temperature variation to land cover and land use intensity changes in China over the last 30 years. Clim Chang 164. https://doi.org/10.1007/s10584-021-02955-y
Jodar J, Carrera J, Cruz A (2010) Irrigation enhances precipitation at the mountains downwind. Hydrol Earth Syst Sc 14(10):2003–2010. https://doi.org/10.5194/hess-14-2003-2010
Kang S, Eltahir EAB (2019) Impact of irrigation on regional climate over eastern China. Geophys Res Lett 46:5499–5505. https://doi.org/10.1029/2019GL082396
Knievel JC, Ahijevych DA, Manning KW (2004) Using temporal modes of rainfall to evaluate the performance of a numerical weather prediction model. Monthly Weather Review 132:2995–3009. https://doi.org/10.1175/MWR2828.1
Kueppers L, Snyder M, Sloan LC (2007) Irrigation cooling effect: Regional climate forcing by land-use change. Geophys Res Lett 34(3):L03703. https://doi.org/10.1029/2006GL028679
Lee X, Goulden ML, Hollinger DY, Barr A, Black TA, Bohrer G (2011) Observed increase in local cooling effect of deforestation at higher latitudes. Nature 479(7373):384–387. https://doi.org/10.1038/nature10588
Li D, Tian PP, Luo HY, Hu TS, Dong B, Cu YL (2020) Impacts of land use and land cover changes on regional climate in the Lhasa River basin, Tibetan Plateau. Sci Total Environ 742:140570. https://doi.org/10.1016/j.scitotenv.2020.140570
Li Y, Zhu LJ, Zhao XY, Li SC, Yan Y (2013) Urbanization impact on temperature change in China with emphasis on land cover change and human activity. J Climate 26:8765–8780. https://doi.org/10.1175/JCLI-D-12-00698.1
Liu GS, Wang WG, Shao QX (2021a) Simulating the climatic effects of irrigation over China by using the WRF-Noah model system with mosaic approach. J Geophys Res Atmos 126(15). https://doi.org/10.1029/2020JD034428
Liu J, Jin J, Niu G-Y (2021b) Effects of irrigation on seasonal and annual temperature and precipitation over China simulated by the WRF model. J Geophys Res Atmos. https://doi.org/10.1029/2020JD03222
Liu TX, Yu LX, Bu K, Yan F, Zhang SW (2018) Seasonal local temperature responses to paddy field expansion from rain-fed farmland in the cold and humid Sanjiang Plain of China. Remote Sensing 10:2009. https://doi.org/10.3390/rs10122009
Liu TX, Yu LX, Zhang SW (2019) Impacts of wetland reclamation and paddy field expansion on observed local temperature trends in the Sanjiang Plain of China. J Geophys Res Earth Surf 124(2):414–426. https://doi.org/10.1029/2018JF004846

Lobell DB, Bonfils CJ, Kueppers LM (2008) Irrigation cooling effect on temperature and heat index extremes. Geophys Res Lett 35:701–705. https://doi.org/10.1029/2008GL034145

Lobell D, Bala G, Mirin A, Phillips T, Maxwell R, Rotman D (2009) Regional Differences in the Influence of Irrigation on Climate. J Clim 22:2248–2255. https://doi.org/10.1175/2008jcli2703.1

Luo P, Mu D, Xue H, Ngo-Duc T, Dang-Dinh K, Takara K, Nover D, Schladow G (2018) Flood inundation assessment for the Hanoi Central Area, Vietnam under historical and extreme rainfall conditions. Sci Rep 8:126623. https://doi.org/10.1038/s41598-018-30024-5

Mao HQ, Yan XD, Xiong Z, Tian HQ (2011) Modeled impact of irrigation on regional climate in India. Acta Ecol Sin 31(4):1038–1045 ((**in Chinese with English abstract**))

Mccarl BA, Attavanich W, Musumba M, Mu J, Aisabokhae R (2014) Land use and climate change. Science 310:1625–1626

Myhre G, Myhre A (2003) Uncertainties in radiative forcing due to suface albedo changes caused by land-use changes. J Clim 16(10):1511–1524. https://doi.org/10.1175/1520-0442-16.10.1511

Nocco MA, Smail RA (2019) Observation of irrigation-induced climate change in the Midwest United States. Glob Change Biol 25:3472–3484. https://doi.org/10.1111/gcb.14725

Pielke RA, Marland G, Betts RA (2002) The influence of land-use changes and landscape dynamics on the climate system: relevance to climate-change policy beyond the radiative effect of greenhouse gases. Philos Trans Royal Soc A Math Phys Eng Sci 360:1705–1719. https://doi.org/10.1098/rsta.2002.1027

Puma M, Cook B (2010) Effects of irrigation on global climate during the 20th century. J Geophys Res 115:D16120. https://doi.org/10.1029/2010JD014122

Sampaio G, Nobre C, Costa MH, Satyamurty P, Soares-Filho BS, Cardoso M (2007) Regional climate change over eastern Amazonia caused by pasture and soybean cropland expansion. Geophys Res Lett 34. L17709-n/a. https://doi.org/10.1029/2007GL030612

Selman C, Misra V (2016) The impact of an extreme case of irrigation on the southeastern United States climate. Climate Dynam 48:1309–1327. https://doi.org/10.1007/s00382-016-3144-1

Shi ZG, Yan XD, Wang ZM (2007) Effects of historical land cover changes on climate[J]. Chin Sci Bull 52(18):2575–2582. https://doi.org/10.1007/s11434-007-0381-z

Skamarock WC, Klemp JB (2008) A time-split nonhydrostatic atmospheric model for weather research and forecasting applications. J Comput Phys 227:3465–3485. https://doi.org/10.1016/j.jcp.2007.01.037

Sorooshian S, Li J, Hsu K-l, Gao X (2011) How significant is the impact of irrigation on the local hydroclimate in California's Central Valley? Comparison of model results with ground and remote-sensing data. J Geophys Res 116. https://doi.org/10.1029/2010jd014775

Su H, Wang W, Jia Y, Han S, Gao H, Niu C (2021) Impact of urbanization on precipitation and temperature over a lake-marsh wetland: a case study in Xiong'an New Area, China. Agric Water Manag 243:106503. https://doi.org/10.1016/j.agwat.2020.106503

Thiery W, Davin EL, Lawrence DM, Hirsch AL, Hauser M, Seneviratne SI (2017) Present-day irrigation mitigates heat extremes. J Geophys Res Atmos 122(3):1403–1422. https://doi.org/10.1002/2016JD025740

Vahmani P, Hogue T (2014) High-resolution land surface modeling utilizing remote sensing parameters and the Noah UCM: a case study in the Los Angeles Basin. Hydrol Earth Syst Sci 18(12):4791–4806. https://doi.org/10.5194/hess-18-4791-2014

Wu L, Feng J, Miao W (2018) Simulating the impacts of irrigation and dynamic vegetation over the North China Plain on regional climate. J Geophys Res Atmos 123(15):8017–8034. https://doi.org/10.1029/2017JD027784

Yan FQ, Yu LX, Yang CB, Zhang SW (2018) Paddy field expansion and aggregation since the mid-1950s in a cold region and its possible causes. Remote Sensing 10(3):384. https://doi.org/10.3390/rs10030384

Yan Y, Tang J, Liu G, Wu J (2019) Effects of vegetation fraction variation on regional climate simulation over Eastern China. Glob Planet Chang 175:173–189. https://doi.org/10.1016/j.gloplacha.2019.02.004

Yu LX, Liu TX, Cai H, Tang J, Bu K, Yan F (2014) Estimating land surface radiation balance using MODIS in northeastern China. J Appl Remote Sens 8(1):083523. https://doi.org/10.1117/1.JRS.8.083523

Yu LX, Liu Y, Liu TX, Yan F (2020) Impact of recent vegetation greening on temperature and precipitation over China. Agric For Meteorol 295:108197. https://doi.org/10.1016/j.agrformet.2020.108197

Yu LX, Yang J, Bu K, Liu T, Jiao Y, Li G (2021) Impacts of saline-alkali land improvement on regional climate: process, mechanisms, and implications. Remote Sensing 13(17):3407. https://doi.org/10.3390/rs13173407

Zhang G, Xiao X, Biradar CM, Dong J, Qin Y, Menarguez MA, Zhou Y, Zhang Y, Jin C, Wang J (2017a) Spatiotemporal patterns of paddy rice croplands in China and India from 2000 to 2015. Sci Total Environ 579:82–92. https://doi.org/10.1016/j.scitotenv.2016.10.223

Zhang X, Xiong Z, Zhang XZ, Shi Y, Liu JY, Shao QQ, Yan XD (2016) Using multi-model ensembles to improve the simulated effects of land use/cover change on temperature: a case study over northeast China. Clim Dynam 46:765–778. https://doi.org/10.1007/s00382-015-2611-4

Zhang LJ, Yu Y, Su LL, Hao TT, Zheng H (2017b) Effects of land use change on air temperature of Heilongjiang Province in 1960–2010. Geogr Sci 37:952–959

Zhao N, Han S, Xu D, Wang J, Yu H (2016) Cooling and wetting effects of agricultural development on Near-Surface atmosphere over Northeast China. Adv Meteorol 1–12. https://doi.org/10.1155/2016/6439276

Zhang L, Wang C, Li X, Zhang H, Li W, Jiang L (2018) Impacts of Agricultural Expansion (1910s–2010s) on the Water Cycle in the Songneng Plain, Northeast China. Remote Sens. https://doi.org/10.3390/rs10071108

Zheng Y, Dong L, Xia Q, Liang C, Wang L, Shao Y (2020) Effects of revegetation on climate in the Mu Us Sandy Land of China. Sci Total Environ 739:139958. https://doi.org/10.1016/j.scitotenv.2020.139958